Desalination and Water Treatment
www.deswater.com

doi: 10.1080/19443994.2015.1137498

57 (2016) 22703–22710
October

Taylor & Francis
Taylor & Francis Group

Synthesis, adsorption and photocatalytic property of halloysite-TiO_2-Fe_3O_4 composites

Pengwu Zheng[a], Yuanyuan Du[a], Dan Liu[b,*], Xiaofei Ma[c]

[a]*School of Pharmacy, Jiangxi Science and Technology Normal University, Nanchang, Jiangxi 330013, China, Tel. +86 791 83805385; emails: zhengpw@126.com (P. Zheng), duyuan01@126.com (Y. Du)*
[b]*School of Physics and Materials Engineering, Dalian Nationalities University, Dalian 116600, China, Tel./Fax: +86 411 87656135; email: liudan@dlnu.edu.cn*
[c]*Chemistry Department, School of Science, Tianjin University, Tianjin 300072, China, Tel. +86 22 27406144; email: maxiaofei@tju.edu.cn*

Received 14 July 2015; Accepted 9 December 2015

ABSTRACT

Halloysite-TiO_2-Fe_3O_4 composites were prepared by sequentially depositing anatase TiO_2 and magnetic Fe_3O_4 particles on the halloysite nanotube (HNT) surfaces. HNT-TiO_2 and HNT-TiO_2-Fe_3O_4 composites were characterized by transmission electron microscopy, energy dispersive X-ray spectroscopy, specific surface analyzer, and X-ray diffraction. The surfaces of HNTs were attached with the aggregates of TiO_2 and Fe_3O_4 nanoparticles, the contents of which were calculated to be about 15.2 and 1.5 wt% in HNT-TiO_2-Fe_3O_4. The adsorption and photodegradation of methylene blue (MB) by HNT-TiO_2 and HNT-TiO_2-Fe_3O_4 were studied. HNT-TiO_2-Fe_3O_4 exhibited the faster adsorption process than HNT-TiO_2. The kinetic adsorption followed the pseudo-second-order model and the isotherm data fitted the Langmuir model well. The maximum adsorption capacities of MB were 28.07 and 27.27 mg/g for HNT-TiO_2 and HNT-TiO_2-Fe_3O_4, respectively. HNT-TiO_2-Fe_3O_4 possessed the better removal capability of MB from the aqueous solution than HNT-TiO_2. About 100% MB was removed for HNT-TiO_2-Fe_3O_4 under UV light irradiation for 12 h, in contrast with about 80% MB removal for HNT-TiO_2. HNT-TiO_2-Fe_3O_4 exhibited higher photocatalytic activity for the persistent organic pollutant 4-nitrophenol than HNT-TiO_2. HNT-TiO_2-Fe_3O_4 and can be easily separated from the aqueous solution with the magnetic rather than the filtration or centrifugation.

Keywords: Halloysite; TiO_2; Adsorption; Photocatalytic property

1. Introduction

Halloysite is a clay mineral with the molecular formula of $Al_2Si_2O_5(OH)_4{\cdot}nH_2O$ [1]. The tubular halloysite is formed by rolling of a kaolin sheet, in which most aluminols and siloxane are, respectively, located in the lumen and the external surface of halloysite nanotube (HNT), and a few silanols and aluminols are exposed in the edges of the sheet. HNT has a variety of applications due to the large surface area, hollow nanotube structure, and tunable surface chemistry of HNT [2]. HNT can adsorb cationic dyes [3] and metal ions [4] due to the cationic exchange between Na^+ on HNT and cationic pollutants in water.

*Corresponding author.

HNT has been used as the supports for catalysts. The silver nanoparticles-supported HNT can catalyze the reduction of 4-nitrophenol with $NaBH_4$ in alkaline aqueous solutions [5]. CdS/HNT composites are doped with several metal ions (Zn^{2+}, Bi^{3+}, Cr^{3+}, and Ni^{2+}) in the hydrothermal method. The photocatalytic activity was evaluated by the degradation of tetracycline under visible-light irradiation [6]. HNT is estimated as the template for the preparation of the nanotubes. Silica nanotubes can be fabricated by acid leaching the natural HNTs [7], and have potential application on the light localization and optical devices. Selective modifications are processed between silica and alumina in HNT. The negatively charged urease is loaded inside positively charged HNT lumen [8]. The embedded urease in HNT can catalyze urea to produce CO_3^{2-} ions and deposit $CaCO_3$ in the lumen of HNT. Some biomolecules such as amylose [9] and DNA [10] can wrap HNTs in the non-covalent functionalization to improve the biocompatibility of HNTs. As the adsorbents, HNTs have been tested for the ability to remove methylene blue (MB) [11,12], neutral red [12,13], and Cr(VI) [14] from the aqueous solution.

The treatment and disposal of wastewater is one of the most serious environmental problems in the whole world [15–17]. The effluents containing pollutants must be treated carefully before discharge. The environmentally friendly technologies are adopted to remove the dyes and the persistent organic pollutant from effluents. Among of them, photocatalytic degradation and adsorption are the effective and economic methods. TiO_2 has been extensively investigated as photocatalyst due to good stability, nontoxicity, low cost, and high catalytic activity [18,19]. In this work, TiO_2 was incorporated to HNT to prepare the HNT-TiO_2 composites, and then Fe_3O_4 was introduced to obtain HNT-TiO_2-Fe_3O_4 composites. In the composites, HNT has been proven as a good adsorbent or a support of photocatalyst, TiO_2 can degrade pollutants on HNT under UV light irradiation, and magnetic Fe_3O_4 can make HNT easily separate from the aqueous solution with the magnetic field. The adsorption of MB dye and the photocatalytic degradation of MB dye and 4-nitrophenol (4-NP) by the composites were also investigated in this work.

2. Experimental

2.1. Materials

HNT was obtained from Hunan province, China. MB dye was provided by Tianjin Benchmark Chemical Reagent Co., Ltd. All other reagents were commercially available and of analytical grade.

2.2. Preparation

2.2.1. Preparation of HNT-TiO_2 composites

Tetrabutyl titanate, $Ti(OC_4H_9)_4$ (29 mL) was added in (80 mL) absolute ethanol, and then 12 g acetic acid was added. Three grams of HNT were dispersed in the mixture, and stirred for 1 h at 30℃. The mixture of 6.8 g ammonium nitrate, 24 mL distilled water, and 20 mL ethanol was added dropwise into HNT suspension, and then stirred for 3 h. The obtained gel was stored at the room temperature for 24 h. The product was centrifuged, washed with water at least twice, and oven-dried at 100℃ to obtain HNT-TiO_2 composite. If the ratio of TiO_2/HNT was larger, the adsorption capacity of the HNT-TiO_2 composite was decreased. If the ratio of TiO_2/HNT was less, the photodegradation of the HNT-TiO_2 composite was reduced.

2.2.2. Preparation of HNT-TiO_2-Fe_3O_4 composites

One gram of HNT-TiO_2 was added in a 200 mL solution of 0.16 g $FeSO_4{\cdot}7H_2O$ and 0.26 g $FeCl_3{\cdot}6H_2O$. NH_3H_2O solution (8 mol/L) was added dropwise to produce iron oxides at 65℃ under N_2. The pH of the final suspension was in the range of 10–11. The mixtures were aged at 70℃ for 4 h, and then washed with distilled water. The obtained HNT-TiO_2-Fe_3O_4 composite was dried at 100℃. The superfluous Fe_3O_4 would decrease the adsorption capacity.

2.3. Characterization

HNT-TiO_2 and HNT-TiO_2-Fe_3O_4 aqueous suspensions were dropped onto the copper grid and air dried. The samples were analyzed using a Transmission electron microscope (TEM) JEM-1200EX, and the atomic weight of Ti and Fe for HNT-TiO_2-Fe_3O_4 was recorded with energy dispersive X-ray spectroscopy (EDS).

Nitrogen adsorption–desorption measurements were performed with an Autosorb-1 specific surface area analyzer (Quantachrome Instruments, USA).

HNT-TiO_2 and HNT-TiO_2-Fe_3O_4 were placed in a sample holder for X-ray diffraction (XRD). XRD patterns were recorded in reflection mode in the angular range of 10°–80° (2θ), at ambient temperature, using a Bruker D8-S4 Pioneer operated at a CuKα wavelength of 1.542 Å.

The magnetic properties of HNT-TiO_2-Fe_3O_4 were measured on a vibrating sample magnetometer (LDJ 9600-1, LDJ Electronics Inc., USA).

2.4. Adsorption of MB dye

Adsorption experiments were conducted using glass bottles containing the dye (initial concentration C_0, 37.39 mg/L MB) and 0.1 g/L HNT-TiO_2 (or HNT-TiO_2-Fe_3O_4). The glass bottles were placed on a slow-moving platform shaker and aliquots of approximately 10 mL were taken at different time intervals during the reaction. The dye concentrations of the solutions were analyzed by UV–vis spectrometry and relative dye adsorption vs. reaction time determined at 25℃.

For adsorption isotherm testing, the concentration of the adsorbent was 0.1 g/L and the dye concentration varied from 0.01 to 0.8 mmol/L. These experiments were carried out at 25℃, and all suspensions were shaken on a rotary shaker at 100 rpm to reach the adsorption equilibrium.

2.5. Photodegradation experiments

The photodegradation experiments were carried out after the adsorption equilibrium. When 0.1 g/L HNT-TiO_2 (or HNT-TiO_2-Fe_3O_4) in MB dye (C_0 37.39 mg/L) reached the adsorption equilibrium in the above adsorption experiments, the glass bottles containing them were exposed to UV irradiation. The photodegradation and adsorption were simultaneously carried out too. The glass bottles containing 10 mg HNT-TiO_2 (or HNT-TiO_2-Fe_3O_4) and 10 mL MB dye (C_0 0.1 mmol/L) were exposed to UV irradiation, or stored in the dark at 25℃. The UV light source was a 12 W UV lamp (λ = 365 nm) and the irradiation intensity was approximately 350 μW/cm^2. The absorbance was recorded using a UV–vis spectrometer at some time intervals (about 1 h), and MB concentrations (C_t) were determined.

For the photocatalytic degradation of 4-NP [20], 10 mg HNT-TiO_2 (or HNT-TiO_2-Fe_3O_4) was dispersed in 10 mL 4-NP solution (10 mg/L). They were exposed to UV irradiation, or stored in the dark at 25℃. The UV light source was a 12 W UV lamp (λ = 253 nm). The concentrations of the 4-NP was performed at 318 nm with a UV–vis spectrometer.

The stability of HNT-TiO_2 and HNT-TiO_2-Fe_3O_4 during the photocatalytic process was evaluated by reusing the catalyst for five runs. After each run, the catalyst was separated by the centrifugation for HNT-TiO_2 and the magnet for HNT-TiO_2-Fe_3O_4.

3. Results and discussion

3.1. Characterization of HNT-TiO_2 and HNT-TiO_2-Fe_3O_4

As shown in Fig. 1, the surfaces of HNTs were attached with the aggregates of TiO_2 or Fe_3O_4 nanoparticles, which may be formed from the precipitation followed by a step-like aggregation process. Because Fe^{3+} and Fe^{2+} were added in a small quantity,

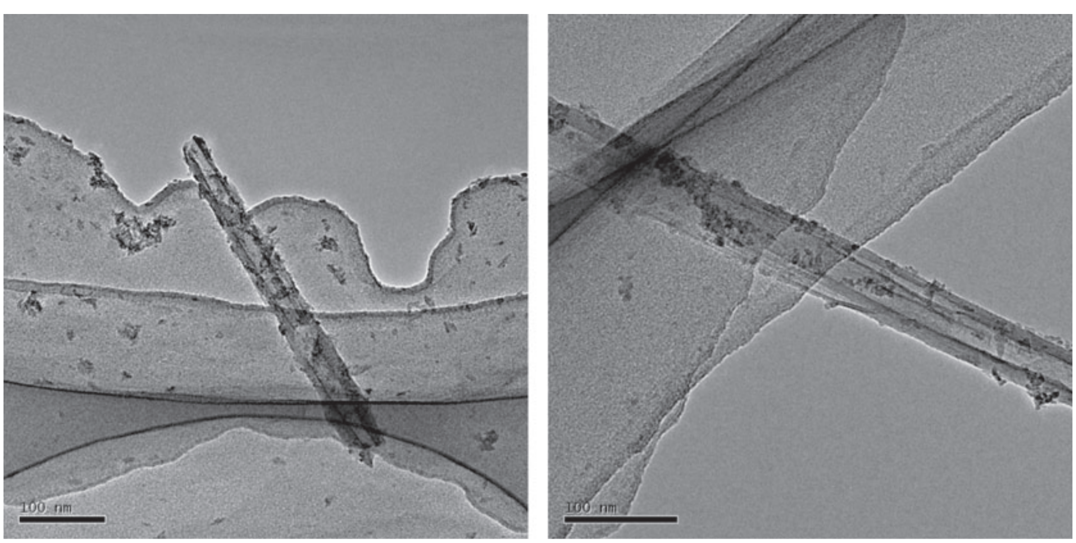

(a) (b)

Fig. 1. TEM micrographs for HNT-TiO_2 (a) and HNT-TiO_2-Fe_3O_4 (b).

and Fe^{3+}/Fe^{2+} could be adsorbed on HNT surfaces by the cationic exchange, Fe_3O_4 particles could form on HNT rather than on the TiO_2 particles.

And the atomic weight of Ti (9.12 wt%) and Fe (1.07 wt%) for HNT-TiO_2-Fe_3O_4 was recorded by EDS in TEM testing. The contents of TiO_2 and Fe_3O_4 particles in HNT-TiO_2-Fe_3O_4 were calculated to be about 15.2 and 1.5 wt%, respectively. In contrast, the atomic weight of Ti for HNT-TiO_2 was 11.36 wt%, so the contents of TiO_2 particles in HNT-TiO_2 were about 18.9 wt%. Obviously, about 20 wt% TiO_2 particles break off from the HNT surface in the process of preparing Fe_3O_4 particles.

The BET surface area of raw HNT was 62.14 m^2/g, while the BET surface areas for HNT-TiO_2 and HNT-TiO_2-Fe_3O_4 were, respectively, 227.72 and 201.19 m^2/g, much higher than that of raw HNT. When TiO_2 particles were attached on HNT, many new surfaces were produced from TiO_2 particles. When Fe_3O_4 particles were further introduced, the BET surface areas decreased. In terms of specific surface areas, the formation of Fe_3O_4 did not counteract the loss of TiO_2 particles. This was consistent with the decreased loading of metal oxide particles of HNT-TiO_2-Fe_3O_4.

The halloysite material was ascribed to Halloysite 7Å, which was characterized and shown in the previous work [3]. In Fig. 2, XRD patterns of HNT-TiO_2 and HNT-TiO_2-Fe_3O_4 were recorded from 10˚ to 80˚ (2θ). HNT-TiO_2 showed characteristic peaks at 2θ values of about 25.2˚, 37.8˚, 47.8˚, 54.5˚, and 62.5˚ [21], as marked in Fig. 2. The XRD patterns of HNT-TiO_2 exhibited all the characteristic reflections of anatase TiO_2. When Fe_3O_4 particles were formed, the powder XRD patterns also displayed distinct peaks at 2θ values of about 30.1, 35.3, 43.2, and 57.2, marked as

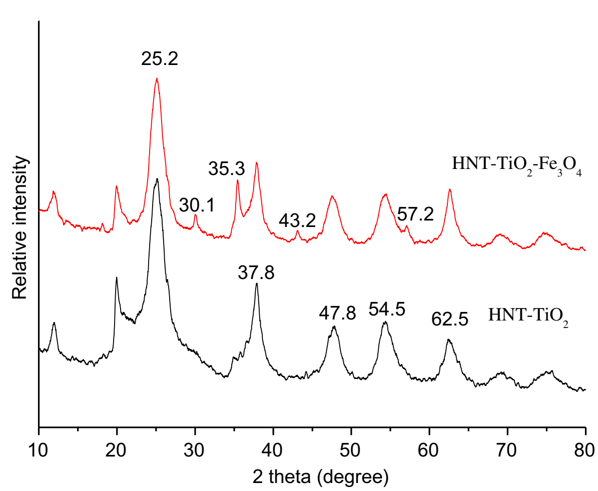

Fig. 2. XRD patterns of HNT-TiO_2 and HNT-TiO_2–Fe_3O_4.

F (2 2 0), F (3 1 1), F (4 0 0), and F (5 1 1) in Fig. 2. These peak positions could correspond to the characteristic peaks of Fe_3O_4 [22].

Fig. 3 shows the magnetic hysteresis curves of HNT-TiO_2-Fe_3O_4 measured at 300 K. HNT-TiO_2-Fe_3O_4 possessed the magnetic properties with the saturation magnetization (2.75 emu/g). Since HNT can be dispersed well in water, the centrifugation and filtration are usually required before testing the absorbance of MB solution or reclaiming the HNT. Now HNT-TiO_2-Fe_3O_4 can easily separate from the aqueous solution with the magnetic.

3.2. MB adsorption

3.2.1. Batch adsorption kinetic modeling

Fig. 4(a) reveals the effect of contact times on adsorption of MB by HNT-TiO_2 and HNT-TiO_2-Fe_3O_4. The amount of adsorbed MB dye for HNT-TiO_2-Fe_3O_4 is higher than that for HNT-TiO_2 at any time.

The adsorption process was investigated in the pseudo-second-order kinetic model, which is expressed as [23]:

$$\frac{t}{q_t} = \frac{1}{k q_e^2} + \frac{t}{q_e} \tag{1}$$

where q_t (mg/g) is the amount of dye adsorbed at any time t (h), k (mg/g h) represents the second-order rate constant, and q_e (mg g^{-1}) is the amount of dye adsorbed at equilibrium. Some kinetic constants from pseudo-second-order model were estimated from the experimental data in Fig. 4(b), and listed in Table 1. The adsorption process for HNT-TiO_2 and HNT-TiO_2-Fe_3O_4 could fit well the pseudo-second-order model with high linear relationship between t/q_t and t ($R > 0.994$). The second-order rate constant k and q_e were obtained from the intercept and slope of the line in a t/q_t vs. t plot. In terms of k, HNT-TiO_2-Fe_3O_4 demonstrated higher values than HNT-TiO_2, and HNT-TiO_2-Fe_3O_4 exhibited the faster adsorption process in Fig. 4(a). Fe_3O_4 particles synchronously bring the magnetism to HNT-TiO_2 and faster adsorption of MB dye.

3.2.2. Batch adsorption isotherm modeling

The adsorption isotherm for MB by HNT-TiO_2 and HNT-TiO_2-Fe_3O_4 is shown in Fig. 5. At very low values of the equilibrium concentration (C_e), q_e changed much with the increasing of C_e, while q_e changed a little at the high C_e (>2 mg/L). The Langmuir model was used to study the adsorption isotherm of MB dye by HNT-TiO_2

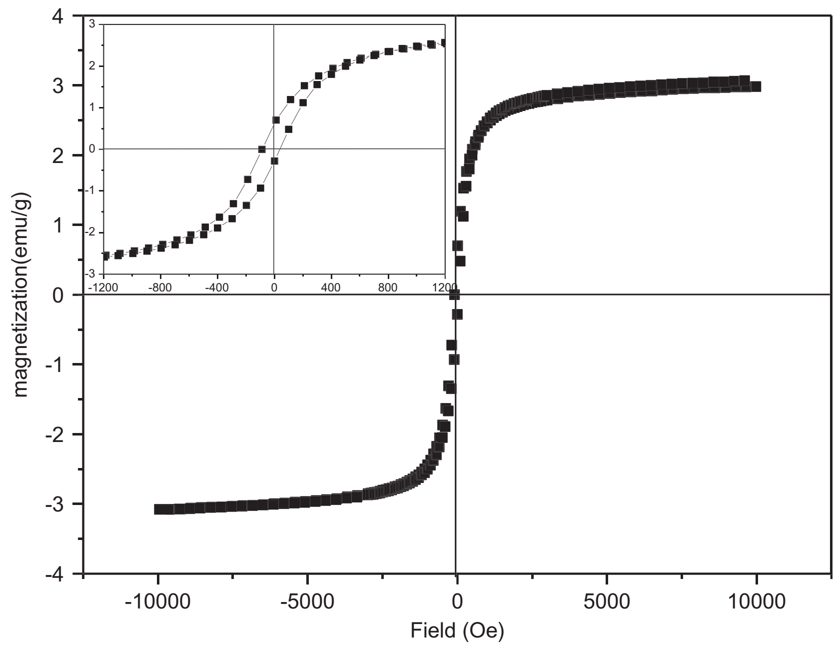

Fig. 3. Hysteresis loops of HNT-TiO_2-Fe_3O_4 measured at 300 K.

or HNT-TiO_2-Fe_3O_4, and determine the maximum monolayer adsorption capacities, q_{max} (mg/g).

The equation is as follows [23]:

$$\frac{C_e}{q_e} = \frac{1}{b\,q_{max}} + \frac{C_e}{q_{max}} \quad (2)$$

where b (L/mg) is the Langmuir adsorption equilibrium constant.

The parameters from Langmuir isotherm are obtained and listed in Table 1. It was exhibited that the adsorption of HNT-TiO_2 and HNT-TiO_2-Fe_3O_4 fit the Langmuir model well because of $R \approx 1$. According to the Langmuir isotherm model, the maximum monolayer adsorption capacities (q_{max}) were 28.07 and 27.27 mg/g for HNT-TiO_2 and HNT-TiO_2-Fe_3O_4, respectively. The q_{max} value of HNT-TiO_2-Fe_3O_4 was very close to HNT-TiO_2. The q_{max} values of HNT-TiO_2 and HNT-TiO_2-Fe_3O_4 were larger than halloysite-Fe_3O_4 (18.64 mg/g) [12].

3.3. Photodegradation

Due to nontoxicity, strong oxidizing power and stability, TiO_2 exhibits excellent photocatalytic properties for the decomposition of a great variety of organic pollutants. TiO_2/clay mineral composites have attracted growing interest due to their strong adsorption of organic pollutants and good degradation properties [20].

HNT-TiO_2 and HNT-TiO_2-Fe_3O_4 adsorbed enough MB dye and reached the adsorption equilibrium. MB adsorption could be neglected in the next process of MB removal. These suspensions were exposed with UV irradiation to reveal the effect of exposure times on the photodegradation of MB dye, as shown in Fig. 6. Since TiO_2 could degrade MB dye with the N-demethylation by in a stepwise process in UV irradiation [24], the maximal absorbance was gradually decreased at 662 nm. The absorbance of MB solution was decreased about 54% after 10 h under UV light irradiation in the presence of HNT-TiO_2, while that was 78% for HNT-TiO_2-Fe_3O_4. HNT-TiO_2-Fe_3O_4 seemed to exhibit the more excellent photocatalytic activity as compared to that of HNT-TiO_2. However, TiO_2 content in HNT-TiO_2-Fe_3O_4 is lower than that in HNT-TiO_2. Therefore, the fast adsorption of HNT-TiO_2-Fe_3O_4 should be considered, when the photodegradation of MB occurred on HNT and the chemical sites for adsorbing MB dye were empty.

Fig. 7 displays the removal of MB dye in the UV irradiation or in the dark. The photolysis of MB was negligible in the dark. When HNT-TiO_2 and HNT-TiO_2-Fe_3O_4 were stored in the dark, C_t decreased gradually. At 12 h, HNT-TiO_2 removed about 47% MB, while HNT-TiO_2-Fe_3O_4 removed about 51% MB. The faster removal of MB dye was consistent with the faster adsorption for HNT-TiO_2-Fe_3O_4 than HNT-TiO_2.

When HNT-TiO_2 and HNT-TiO_2-Fe_3O_4 were exposed under UV light irradiation, both of them

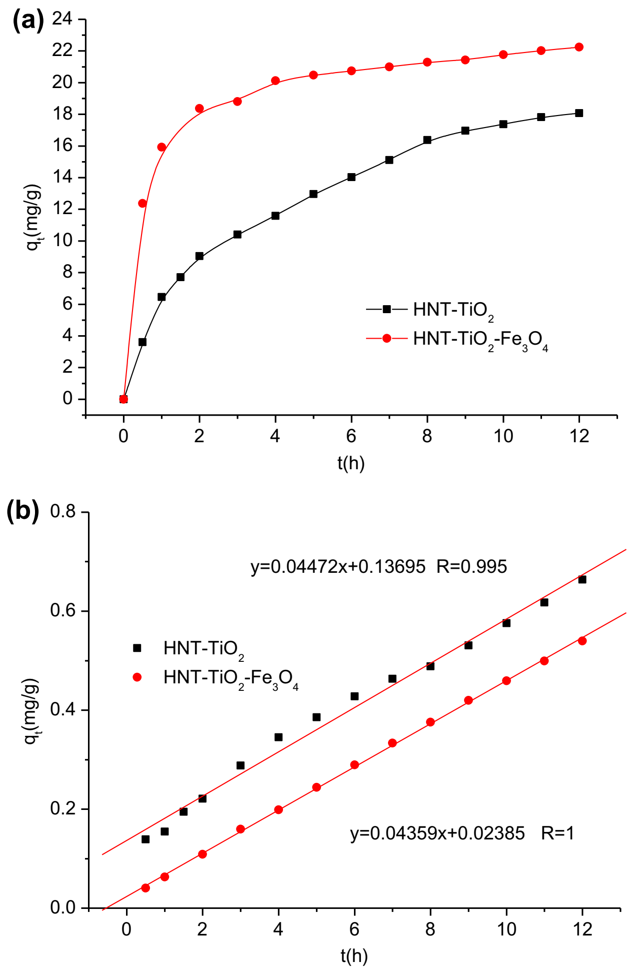

Fig. 4. Effect of contact time on adsorption of MB (a) and the pseudo-second-order mode (b) for batch adsorption of MB by HNT-TiO_2 and HNT-TiO_2-Fe_3O_4 at 25˚C. Initial concentration: MB 37.39 mg/L; HNT-TiO_2 or HNT-TiO_2-Fe_3O_4 0.1 g/L.

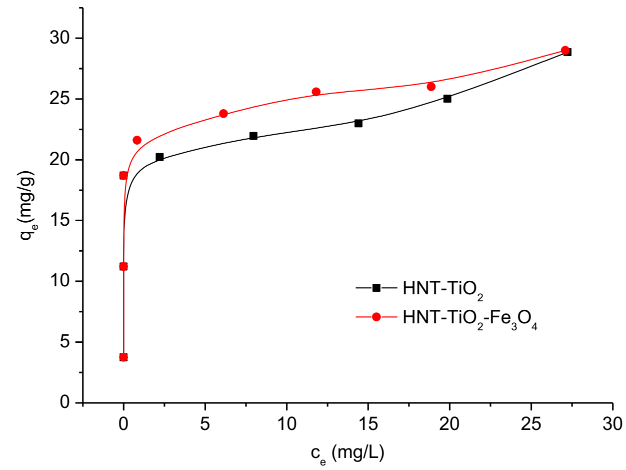

Fig. 5. Adsorption isotherms of MB onto HNT-TiO_2 and HNT-TiO_2-Fe_3O_4 at 25˚C. HNT-TiO_2 or HNT-TiO_2-Fe_3O_4 0.1 g/L.

exhibited better removal of MB dye than those in the dark. The removal of MB dye actually came from both the adsorption from HNT and the photodegradation from photocatalyst TiO_2. HNT-TiO_2-Fe_3O_4 exhibited the excellent removal of MB. When the equilibrium reached at 12 h, about 100% MB was removed for HNT-TiO_2-Fe_3O_4 under UV light irradiation, in contrast with about 80% MB removal for HNT-TiO_2. (In the work of Yu et al. [25], only 31.4% of the absorbed MB desorbed from the biosorbent with TiO_2 hydrosol.) The more removal of MB dye was mainly ascribed to the faster adsorption of HNT-TiO_2-Fe_3O_4, because the content of TiO_2 with photocatalytic activity was lower in HNT-TiO_2-Fe_3O_4 than HNT-TiO_2, and iron oxide exhibited little photocatalytic activity for the decomposition of MB.

To further evaluate the photocatalytic properties of HNT-TiO_2-Fe_3O_4 and HNT-TiO_2, the removal of 4-NP was studied. 4-NP is a toxic organic pollutant and difficult to decompose. Fig. 8 shows the removal of 4-NP by HNT-TiO_2 and HNT-TiO_2-Fe_3O_4 in the UV irradiation or in the dark. Since the removal of 4-NP in the dark was very low, HNT-TiO_2 and HNT-TiO_2-Fe_3O_4 had the poor ability to absorb 4-NP. The adsorption of 4-NP was not studied. In the UV irradiation, HNT-TiO_2 and HNT-TiO_2-Fe_3O_4 exhibited good photodegradation of 4-NP. When 4-NP was exposed for 4.5 h in UV irradiation, about 91 and 97% of 4-NP was

Table 1
Constants of pseudo-second-order model and Langmuir model for MB adsorption by HNT-TiO_2 and HNT-TiO_2-Fe_3O_4 at 25˚C

	Pseudo-second-order model			Langmuir model		
	k (g/mg h)	q_e (mg/g)	R	q_{max} (mg/g)	b (L/mg)	R
HNT–TiO_2	0.0146	22.36	0.995	28.07	2.55	0.991
HNT-TiO_2-Fe_3O_4	0.0797	22.94	1	27.27	1.40	0.993

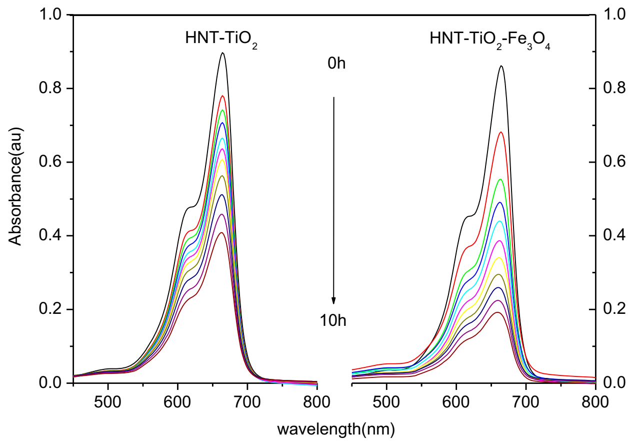

Fig. 6. The UV–vis absorption spectra of the MB solution during the photocatalytic degradation in the presence of HNT-TiO_2 or HNT-TiO_2-Fe_3O_4 under UV light irradiation.

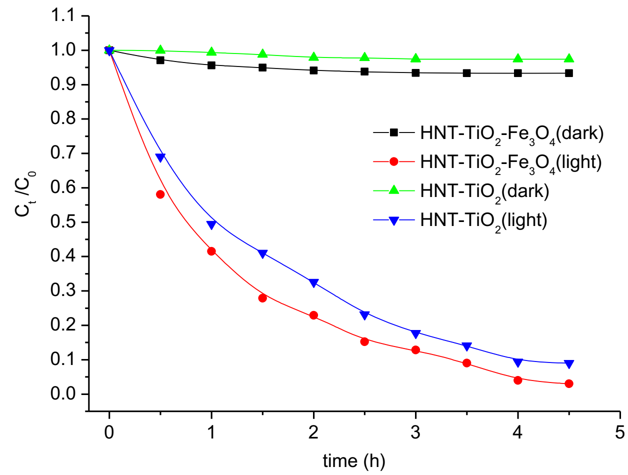

Fig. 8. Photocatalytic degradation of 4-NP by HNT-TiO_2 and HNT-TiO_2-Fe_3O_4.

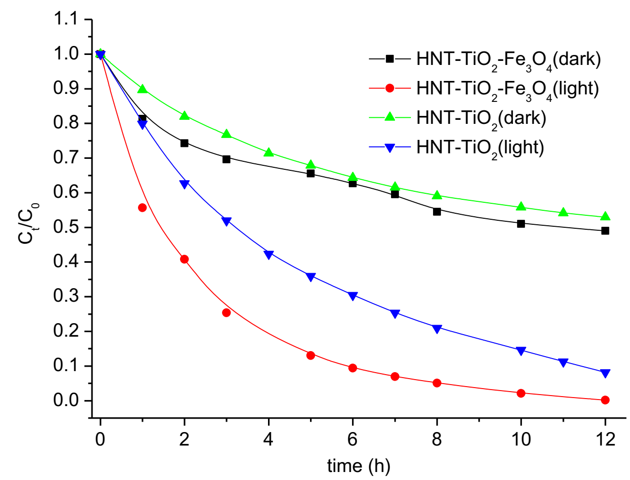

Fig. 7. Photocatalytic degradation in the UV irradiation and adsorption in the dark of MB dye by HNT-TiO_2 and HNT-TiO_2-Fe_3O_4.

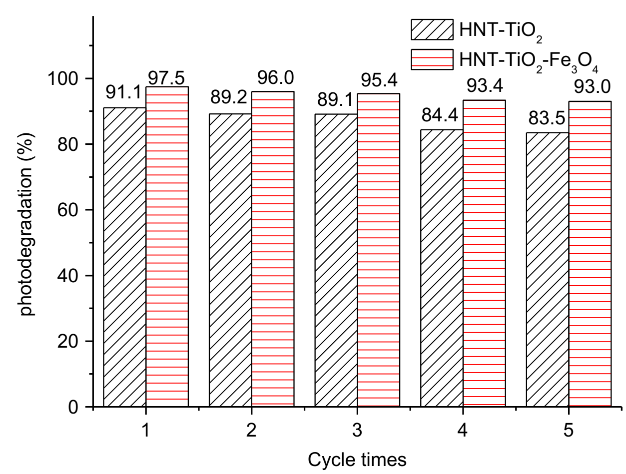

Fig. 9. The stability of HNT-TiO_2 and HNT-TiO_2-Fe_3O_4 after five cycles of photocatalytic decomposition of 4-NP.

removed for HNT-TiO_2 and HNT-TiO_2-Fe_3O_4, respectively. And the introduction of iron oxide increased the removal of 4-NP.

To evaluate the stability, HNT-TiO_2 and HNT-TiO_2-Fe_3O_4 were reused for five runs of photodegradation of 4-NP under UV light. As shown in Fig. 9, both of them had not significant loss of photocatalytic activity after five recycles. The degradation efficiency decreased from 91 to 83.5% for HNT-TiO_2, while the degradation efficiency decreased from 97.5 to 93% for HNT-TiO_2-Fe_3O_4. This result indicates that HNT-TiO_2-Fe_3O_4 remained more effective and stable than HNT-TiO_2 under successive UV light.

4. Conclusions

TiO_2 and Fe_3O_4 nanoparticles were deposited on HNT to obtain magnetic HNT-TiO_2-Fe_3O_4 composites. Fe_3O_4 particles synchronously bring the magnetism to HNT-TiO_2 and faster adsorption of MB dye. This could be related to that the introduction of Fe_3O_4 decreased the loading of metal oxides on HNT surfaces, and resulted in the fewer impediments for MB adsorption.

The kinetic adsorption and the isotherm data respectively fit the pseudo-second-order and the Langmuir model well. The maximum adsorption capacities of MB were 28.07 and 27.27 mg/g for HNT-TiO_2 and HNT-TiO_2-Fe_3O_4, respectively. HNT-TiO_2-Fe_3O_4 exhibited the excellent removal of MB, which can remove about 100% MB dye under UV light irradiation for 12 h. The removal of MB dye was ascribed to both the adsorption from HNT and the photodegradation from photocatalyst TiO_2, but the adsorption played more important role than the photodegradation. The introduction of iron oxide increased the removal of 4-NP due to photocatalytic degradation, and the adsorption process of 4-NP can be ignored. And HNT-TiO_2-Fe_3O_4 can be magnetically separated from the solution, and repeatedly used for photodegradation of 4-NP.

Acknowledgments

This research was supported by the Science and Technology Project of Jiangxi Provincial Office of Education under Grant KJLD12082; the Fundamental Research Funds for the Central Universities under Grant DC201502080402 and the Scientific Research Fund of Liaoning Provincial Education Department under Grant L2013505.

References

[1] M.X. Liu, B.C. Guo, Q.L. Zou, M.L. Du, D.M. Jia, Interactions between halloysite nanotubes and 2, 5-bis (2-benzoxazolyl) thiophene and their effects on reinforcement of polypropylene/halloysite nanocomposites, Nanotechnology 19 (2008) 205709.

[2] W.O. Yah, A. Takahara, Y.M. Lvov, Selective modification of halloysite lumen with octadecylphosphonic acid: New inorganic tubular micelle, J. Am. Chem. Soc. 134 (2012) 1853–1859.

[3] Y.Y. Du, P.W. Zheng, Adsorption and photodegradation of methylene blue on TiO_2-halloysite adsorbents, Korean J. Chem. Eng. 31 (2014) 2051–2056.

[4] A.F. Ismail, S.A. Hashemifard, T. Matsuura, Facilitated transport effect of Ag^+ ion exchanged halloysite nanotubes on the performance of polyetherimide mixed matrix membrane for gas separation, J. Membr. Sci. 379 (2011) 378–385.

[5] P. Liu, M.F. Zhao, Silver nanoparticle supported on halloysite nanotubes catalyzed reduction of 4-nitrophenol (4-NP), Appl. Surf. Sci. 255 (2009) 3989–3993.

[6] W.N. Xing, L. Ni, X.L. Liu, Y.Y. Luo, Z.Y. Lu, Y.S. Yan, P.W. Huo, Effect of metal ion (Zn^{2+}, Bi^{3+}, Cr^{3+}, and Ni^{2+})-doped CdS/halloysite nanotubes (HNTs) photocatalyst for the degradation of tetracycline under visible light, Desalin. Water Treat. 53 (2015) 794–805.

[7] Y. Zhang, L.J. Fu, H.M. Yang, Insights into the physicochemical aspects from natural halloysite to silica nanotubes, Colloids Surf., A: Physicochem. Eng. Aspects 414 (2012) 115–119.

[8] D.G. Shchukin, G.B. Sukhorukov, R.R. Price, Y.M. Lvov, Halloysite nanotubes as biomimetic nanoreactors, Small 1 (2005) 510–513.

[9] P.R. Chang, Y.F. Xie, D.L. Wu, X.F. Ma, Amylose wrapped halloysite nanotubes, Carbohydr. Polym. 84 (2011) 1426–1429.

[10] M.H. Shamsi, K.E. Geckeler, The first biopolymer-wrapped non-carbon nanotubes, Nanotechnology 19 (2008) 075604.

[11] M.F. Zhao, P. Liu, Adsorption behavior of methylene blue on halloysite nanotubes, Microporous Mesoporous Mater. 112 (2008) 419–424.

[12] Y.F. Xie, D.Y. Qian, D.L. Wu, X.F. Ma, Magnetic halloysite nanotubes/iron oxide composites for the adsorption of dyes, Chem. Eng. J. 168 (2011) 959–963.

[13] P. Luo, Y.F. Zhao, B. Zhang, J.D. Liu, Y. Yang, J.F. Liu, Study on the adsorption of Neutral Red from aqueous solution onto halloysite nanotubes, Water Res. 44 (2010) 1489–1497.

[14] J.H. Wang, X. Zhang, B. Zhang, Y.F. Zhao, R. Zhai, J.D. Liu, R.F. Chen, Rapid adsorption of Cr(VI) on modified halloysite nanotubes, Desalination 259 (2010) 22–28.

[15] J.L. Gong, B. Wang, G.M. Zeng, C.P. Yang, C.G. Niu, Q.Y. Niu, W.J. Zhou, Y. Liang, Removal of cationic dyes from aqueous solution using magnetic multi-wall carbon nanotube nanocomposite as adsorbent, J. Hazard. Mater. 164 (2009) 1517–1522.

[16] K. Belkassa, F. Bessaha, K. Marouf-Khelifa, I. Batonneau-Gener, J. Comparot, A. Khelifa, Physicochemical and adsorptive properties of a heat-treated and acid-leached Algerian halloysite, Colloids Surf., A: Physicochem. Eng. Aspects 421 (2013) 26–33.

[17] Z.G. Jia, J.H. Liu, Q.Z. Wang, M.F. Ye, R.S. Zhu, Facile preparation of mesoporous nickel oxide microspheres and their adsorption property for methyl orange from aqueous solution, Mater. Sci. Semicond. Process. 26 (2014) 716–725.

[18] H.Q. Wang, X.L. Liu, X.L. Liu, P.W. Huo, Q.F. Guan, Preparation of polypyrrole-TiO_2 and its adsorption and photocatalytic degradation of salicylic acid, Desalin. Water Treat. 54 (2015) 3291–3299.

[19] R.R. Kalantary, Y.D. Shahamat, M. Farzadkia, A. Esrafili, H. Asgharnia, Photocatalytic degradation and mineralization of diazinon in aqueous solution using nano-TiO 2 (Degussa, P25): Kinetic and statistical analysis, Desalin. Water Treat. 55 (2015) 555–563.

[20] Y.L. Zhang, Y.D. Guo, G.K. Zhang, Y.Y. Gao, Stable TiO_2/rectorite: Preparation, characterization and photocatalytic activity, Appl. Clay Sci. 51 (2011) 335–340.

[21] D. Papoulis, S. Komarneni, D. Panagiotaras, E. Stathatos, D. Toli, K.C. Christoforidis, M. Fernández-García, H. Li, S. Yin, T. Sato, H. Katsuki, Halloysite-TiO_2 nanocomposites: Synthesis, characterization and photocatalytic activity, Appl. Catal. B: Environ. 132–133 (2013) 416–422.

[22] Z.G. Liu, F.S. Zhang, R. Sasai, Arsenate removal from water using Fe_3O_4- loaded activated carbon prepared from waste biomass, Chem. Eng. J. 160 (2010) 57–62.

[23] V.K. Saini, M.L. Pinto, J. Pires, Synthesis and adsorption properties of micro/mesoporous carbon-foams prepared from foam-shaped sacrificial templates, Mater. Chem. Phys. 138 (2013) 877–885.

[24] J.M. Wang, C. Li, H. Zhuang, J.H. Zhang, Photocatalytic degradation of methylene blue and inactivation of Gram-negative bacteria by TiO_2 nanoparticles in aqueous suspension, Food Control 34 (2013) 372–377.

[25] J.X. Yu, R.A. Chi, J. Guo, Y.F. Zhang, Z.G. Xu, C.Q. Xiao, Desorption and photodegradation of methylene blue from modified sugarcane bagasse surface by acid TiO_2 hydrosol, Appl. Surf. Sci. 258 (2012) 4085–4090.